PCCP

PAPER

Kinetics and mechanism of the reaction of OH with the trimethylbenzenes – experimental evidence for the formation of adduct isomers†

Birger Bohn[*a] and **Cornelius Zetzsch**[bc]

The reversible gas-phase addition of OH radicals to the trimethylbenzenes was investigated in pulsed experiments utilizing VUV flash-photolysis resonance-fluorescence of H_2O in the temperature range of 275–340 K. Triexponential OH decays were observed in the presence of the trimethylbenzenes, indicating the participation of more than one adduct species. Analytical solutions for the system of differential equations with two adduct isomers were derived, and the OH decay curves were evaluated based on this reaction model. This led to significant improvements of fit qualities and notable changes in OH rate constants compared to a previous model with a single adduct species. The detailed analysis was confined to 1,3,5-trimethylbenzene where reversible formation of two OH-aromatic *ortho*- and *ipso*-adduct isomers is feasible in accordance with the extended reaction model. Only after inclusion of additional isomerization reactions, consistent thermochemical data were obtained from the fitted rate constants. Reaction enthalpies of -83 ± 7 kJ mol^{-1} and -35 ± 22 kJ mol^{-1} were derived for the formation of one adduct isomer and the isomerization into the other, respectively. Based on literature data, the more and less stable adducts were assigned to *ipso*- and *ortho*-adduct isomers, respectively. The potential isomerization precluded the determination of primary yields of adduct isomers but formation of the *ipso*-adduct in any case is a minor process. For the rate constants of the OH + 1,3,5-trimethylbenzene reaction an Arrhenius expression $k_{OH} = 1.32 \times 10^{-11}$ cm^3 s^{-1} exp(450 $\pm$ 50 K/T) was obtained. Based on the same approach, the rate constants of the OH reactions with 1,2,3-trimethylbenzene and 1,2,4-trimethylbenzene were derived as $k_{OH} = 3.61 \times 10^{-12}$ cm^3 s^{-1} exp(620 $\pm$ 80 K/T) and $k_{OH} = 2.73 \times 10^{-12}$ cm^3 s^{-1} exp(730 $\pm$ 70 K/T), respectively.

1 Introduction

Aromatic compounds are important anthropogenic polluters of the urban atmosphere affecting air quality by secondary formation of ozone and particulate matter. The gas-phase degradation of aromatics under atmospheric conditions is mainly initiated by reactions with OH radicals followed by secondary reactions with O_2 leading to ring-cleavage products (unsaturated carbonyl compounds, glyoxals and epoxides) or oxidized ring-retaining products (phenols, benzaldehydes).[1–3] The initial steps of the oxidation processes have been studied for a number of aromatic compounds under laboratory and simulation chamber conditions. However, many details regarding the product yields of the different reaction pathways are still uncertain.

The initial OH reaction mainly proceeds by addition, forming an OH-aromatic adduct. Owing to the stability of the aromatic ring this adduct is unstable and the addition is markedly reversible, at least above room temperature. Although the reversibility is unimportant in the atmosphere because of fast competing reactions, by observing OH in equilibrium with the adduct kinetic information on the formation and fate of the adduct can be derived which is of fundamental interest in understanding the oxidation mechanisms of aromatic compounds. For example, in experiments with pulsed OH formation in the presence of aromatics, the reversible addition leads to complicated OH decay curves.[4–7] In previous studies these OH decay curves were analysed in terms of a kinetic model assuming that a single adduct species is formed as in the case of benzene. The corresponding analytical solution then

[a] *Institut für Energie- und Klimaforschung IEK-8: Troposphäre, Forschungszentrum Jülich GmbH, 52425 Jülich, Germany. E-mail: b.bohn@fz-juelich.de; Fax: +49 2461 615346*
[b] *Atmospheric Chemistry Research Laboratory, University of Bayreuth, 95448 Bayreuth, Germany*
[c] *Fraunhofer Institute for Toxicology and Experimental Medicine, 30625 Hannover, Germany*

This journal is © the Owner Societies 2012

Phys. Chem. Chem. Phys., 2012, **14**, 13933–13948 | 13933

predicts biexponential OH decay curves (sum of two exponential decays) that were fitted to the experimental data to extract rate constants for reactions of both OH and the adduct.[4,5] Moreover, because data analysis of biexponential decay curves is not as straightforward as for monoexponential decays, advanced tools were developed that allowed us to fit whole sets of curves obtained at different reactant concentrations simultaneously. This method was applied successfully for a number of aromatic compounds.[6,7] An important finding was that the adduct $+ O_2$ reactions are the dominant secondary reactions under typical atmospheric conditions.[6,7]

However, except for a few selected compounds, the assumption of a single adduct species is a simplification. Typically several adduct isomers can be formed. For example, for the series of methyl-substituted monocyclic aromatic compounds carrying one to six CH_3-groups, only hexamethylbenzene is expected to form strictly one adduct isomer, an *ipso*-adduct in this case.[7] All other compounds can form two or more structural isomers with a maximum of six in the case of 1,2,4-trimethylbenzene, not considering stereoisomers with identical thermochemical properties. In principle this is expected to lead to highly complicated, multiexponential OH decay curves. Nevertheless, OH decay curves mostly turned out to be effectively biexponential within experimental error. This can be explained by similar properties of different isomers, a dominant formation of one isomer, or fast isomerizations. An example is toluene where no deviation from biexponential behaviour was observed[6] although four possible isomers can be formed by OH addition at *ortho*-, *meta*-, *para*-, and *ipso*-positions with respect to the CH_3-group. More recently we noticed deviations from biexponential behaviour in the case of 1,3,5-trimethylbenzene in the data set examined in this work, but no quantitative evaluation was attempted.[7]

Before about ten years ago, *ipso*-type adducts, where the OH adds at an already substituted position at the aromatic ring, were hardly considered in the gas-phase reaction mechanism. At that time theoretical work predicted significant yields for the *ipso*-adduct of toluene.[8] Moreover, the rate constant of the OH + hexamethylbenzene reaction was shown to be extremely fast and inconsistent with the expected, slow rate constant for the H-atom abstraction reaction from the CH_3-substituent groups.[9] Reversible formation of an adduct in the OH + hexamethylbenzene reaction was confirmed in the meantime and the adduct $+ O_2$ reaction was studied by the method outlined above.[7] The latter two studies established the existence of *ipso*-type adducts experimentally, at least for the fully substituted hexamethylbenzene. As a consequence, the number of potentially significant isomers increased for substituted aromatic compounds but the actual yields of different isomers remain widely unknown.

The measurements with trimethylbenzenes (TMB) analysed in this work were already made several years ago. A former analysis based on the usual assumption of one adduct species was not satisfactory and for that reason the results were not published previously with the exception of the rate constants of the OH + TMB reactions for the three isomers 1,3,5-, 1,2,3- and 1,2,4-TMB that were released in the form of temperature dependent parameterizations.[10] These results are revised in this work. The possibility that adduct isomers were responsible for the problems with the data analysis was not considered in the former evaluation because at least for the symmetric 1,3,5-TMB no adduct isomers were expected neglecting formation of *ipso*-adducts. Moreover, the concept of considering more than one adduct isomer in the analysis had not yet been developed.

In this work an extended kinetic model considering two adduct isomers will be introduced and applied in a re-analysis of the previously obtained experimental data with 1,3,5-TMB[10] based on analytical solutions. We will show that this leads to an improved description of the data consistent with formation of two adduct isomers. The same procedure was also applied to the previously obtained data with 1,2,3-TMB and 1,2,4-TMB to correct the OH rate constants.[10] Although the number of possible adduct isomers is greater than two for these compounds, the improvement of data description by the extended model was comparable, justifying this approach.

2 Experimental

The flash-photolysis/resonance fluorescence (FP/RF) apparatus used in this work is based on work by Stuhl and Niki[11,12] and subsequent developments.[4,5] A FP/RF cell with efficient, anti-reflection coated quartz optics, partly automated pulsed photolysis, as well as digital data acquisition and evaluation by a programmable microprocessor (FLEXTRAN, Tracor, and LSI 11/2, Digital Equipment Corporation) was developed by Wahner and Zetzsch.[4] The FP/RF cell with similar optics and dimensions but variable temperature, used in the present study, has been constructed and employed by Witte *et al.*[5] The RF sensitivity was further improved by placing the microwave discharge into the focus of the optics, and convenient software was developed for automated controlling and monitoring of the whole experiment (flash lamp, electronic mass flow controllers, magnetic valves, temperature, total pressure, partial pressures of water as a precursor of OH and reactant). A detailed description of the setup was given by Koch *et al.*[7]

OH radicals were produced in helium buffer gas by pulsed VUV flash-photolysis of water vapour in a thermostated reaction volume. OH was continuously excited electronically by OH fluorescence around 308 nm from an attached microwave discharge lamp running with argon and added water vapour. After passing an interference filter, fluorescence from the reaction volume was detected by a photomultiplier mounted at right angles to the flash lamp and the resonance lamp. Photomultiplier signals were recorded using the photon counting technique with a multichannel scaler board. Typically 150–300 single experiments were accumulated to obtain sufficient intensity for a proper evaluation of the decay curves. Background was recorded for up to 5 s and pulse repetition rates were 0.2 Hz. Background count rates ranged around 40 kHz while typical OH starting count rates were 50 kHz. With 150–300 single measurements this resulted in S/N-ratios of 70–100 at starting interval widths of 1.2 ms.

In order to remove high-frequency noise and avoid unnecessary large data files, the data originally recorded by the multichannel scaler were re-binned using interval widths that increased with reaction time following a verified algorithm.[7,13] By this data compression the original 4096 data points were condensed to 61 values for each decay curve that were roughly equidistant

Table 1 Summary of experimental conditions and biexponential model-1 fit results for experiments with 1,3,5-TMB. Left: Temperatures T, total pressures p of He, range of reactant concentrations, and the number m of OH decay curves recorded. Right: Model-1 fit results and estimated error limits from simultaneous fits to the m decay curves at different aromatics concentrations

#	T/K	p/hPa	[Aromatic]/10^{12} cm^{-3}	m	k_2/s^{-1}	$k_{1a} + k_{1b}$/10^{-11} cm^3 s^{-1}	$k_{1a}k_{-1a}$/10^{-10} cm^3 s^{-2}	$k_{-1a} + k_3$/s^{-1}	DOF	χ^2/DOF
1	276.3	380	1.0–5.7	6	19.6 ± 6.1	$6.82 \pm^{0.42}_{0.40}$	$0.43 \pm^{0.47}_{0.25}$	$4.2 \pm^{11}_{3.3}$	350	1.17
2	282.8	380	1.0–5.7	10	16.2 ± 4.8	$6.54 \pm^{0.37}_{0.35}$	$0.81 \pm^{0.27}_{0.22}$	$4.5 \pm^{2.1}_{1.5}$	586	1.11
3	288.1	750	1.0–6.7	7	10.4 ± 6.0	$6.40 \pm^{0.43}_{0.40}$	$1.20 \pm^{0.46}_{0.33}$	$5.1 \pm^{2.9}_{1.8}$	409	1.16
4	293.4	750	1.0–5.7	6	9.1 ± 4.1	$6.11 \pm^{0.31}_{0.30}$	$1.75 \pm^{0.30}_{0.27}$	$6.3 \pm^{1.2}_{1.0}$	350	1.06
5	298.9	380	0.9–5.8	7	14.5 ± 2.8	$5.77 \pm^{0.24}_{0.23}$	$2.48 \pm^{0.22}_{0.20}$	$6.4 \pm^{0.5}_{0.5}$	409	1.60
6	299.1	750	0.5–5.3	7	9.8 ± 1.1	$5.76 \pm^{0.20}_{0.20}$	$2.57 \pm^{0.21}_{0.20}$	$7.1 \pm^{0.5}_{0.5}$	409	1.57
7	304.4	380	0.9–5.7	7	10.2 ± 1.8	$5.62 \pm^{0.23}_{0.22}$	$4.16 \pm^{0.30}_{0.28}$	$10.0 \pm^{0.6}_{0.5}$	409	1.79
8	313.9	380	0.9–5.5	7	9.2 ± 1.0	$5.03 \pm^{0.26}_{0.25}$	$8.44 \pm^{0.70}_{0.65}$	$19.9 \pm^{0.9}_{0.9}$	409	2.98
9	318.4	750	0.5–5.3	7	8.0 ± 0.5	$5.18 \pm^{0.37}_{0.35}$	$13.6 \pm^{1.6}_{1.4}$	$30.6 \pm^{1.7}_{1.6}$	409	2.97
10	323.5	380	0.5–5.2	7	5.5 ± 0.3	$4.62 \pm^{0.51}_{0.46}$	$17.8 \pm^{3.2}_{2.7}$	$43.6 \pm^{3.2}_{3.0}$	409	2.62
11	333.1	380	0.5–5.2	7	5.0 ± 0.3	$3.65 \pm^{0.76}_{0.65}$	$28.2 \pm^{9.7}_{7.3}$	$86.8 \pm^{10}_{9.1}$	409	2.60
12	333.1	750	0.5–5.2	7	4.9 ± 0.2	$3.94 \pm^{0.75}_{0.65}$	$32.9 \pm^{10}_{7.9}$	$93.0 \pm^{9.8}_{8.9}$	409	1.81
13	338.4	750	0.5–5.3	7	5.1 ± 0.2	$3.69 \pm^{0.82}_{0.69}$	$46.4 \pm^{17}_{13}$	$140 \pm^{15}_{15}$	409	2.95
14	340.0	380	0.5–5.1	7	5.3 ± 0.2	$2.88 \pm^{1.04}_{0.80}$	$33.4 \pm^{21}_{14}$	$132 \pm^{25}_{23}$	409	4.20

on a logarithmic time scale. It was tested that this procedure led to no systematic deviations in the subsequently applied curve fitting procedures,[7] but the variable interval width had to be considered explicitly in the data analysis.

Experimental conditions for 1,3,5-trimethylbenzene are summarized in Table 1. Typically seven OH decay curves at different reactant concentrations were recorded for each temperature. Temperatures ranged between 275 K and 340 K. Using calibrated mass flow controllers, the gas-mixture was slowly flowing through the reaction volume to avoid build-up of reaction and photolysis products. Helium was used as a buffer gas to minimize quenching of excited OH. Total pressures of 380 hPa and 750 hPa were employed at total volume flow rates of 1000 and 2000 sccm, respectively. The gas-mixture was entering the reaction cell through a thermostated Woods horn (acting as a radiation trap opposite to the resonance lamp). This resulted in a reduction of flow velocities and effective heat exchange with the thermostated walls of the reaction cell before the gas mixture reached the detection volume. Flow velocities below 1 cm s^{-1} were evaluated for the detection volume.

OH starting concentrations were estimated based on previous work[7,14] and were around 1×10^{10} cm^{-3} at H$_2$O concentrations of typically 4×10^{15} cm^{-3}. Because the OH precursor H$_2$O is unreactive towards OH, experiments were feasible at relatively long time-scales. OH was detectable for up to 1 s, dependent on experimental conditions. Consequently, also low concentrations of added reactants were sufficient ($<6 \times 10^{12}$ cm^{-3}) but pseudo-first order conditions always applied for OH in the presence of the aromatic reactants. Aromatics were introduced by a gas saturation technique where a known flow of buffer gas was fed through a liquid sample of the reactant taking up the vapour pressure at an accurately known temperature of typically 260 K. Vapour pressures of the TMB reactants were calculated using parameterizations from the literature[15] with a stated 4.8% accuracy. For 1,3,5-trimethylbenzene the vapour pressures are confirmed within 2% around 260 K in a more recent compilation.[16] We further estimate a ± 0.3 K accuracy of our temperature measurements that translate to about 5% additional uncertainties of the resulting aromatics concentrations.

Decay curves in the absence of aromatics were not regularly recorded during the measurements because turning on and off of the gas saturation system induced too long waiting times. Test measurements with no added aromatics showed that the pressure and temperature dependence of the background decay rate constants was consistent with those that were extrapolated from the measurements with added aromatics (Section 3.3). However, a minor complication was that OH decays with no added aromatics to some extent remained biexponential most likely because part of the background reactivity was attributable to aromatic compounds. A quantitative explanation of this behaviour is difficult. On the other hand, this unaccounted, slow recycling of OH is negligible upon addition of aromatics when the total OH reactivity was dominated by the added reactants.

Because 1,3,5-TMB is strongly absorbing in a wavelength range below 230 nm, the fraction that can be photolyzed was estimated from a measured spectrum of the flash-lamp.[17] The spectral range considered was limited to > 150 nm because the cut-off of the quartz lens used was around 160 nm and to <290 nm because neither H$_2$O nor 1,3,5-TMB dissociate or absorb in that region. Based on absorption cross sections of H$_2$O from the literature,[18] the spectrum was scaled to match a OH starting concentration of 1×10^{10} cm^{-3}. A photolyzed fraction of 1,3,5-TMB $<1 \times 10^{-4}$ was then obtained using absorption cross sections of 1,3,5-TMB from the literature[19,20] and a maximum quantum yield of unity. Thus, even if the potential photo-fragments, e.g. dimethylbenzyl radicals, are highly reactive towards OH they can hardly compete with the large excess of 1,3,5-TMB, a quite reactive compound by itself.

Nevertheless, radical–radical reactions following the initial formation of OH radicals and H-atoms in the H$_2$O photolysis may contribute to the final loss of OH and OH-aromatic adducts from the detection volume. Because radical concentrations were low, these processes were not considered explicitly and were assumed to be incorporated in first-order background loss rate constants of all radical species. The same applies for diffusion processes. Based on numerical simulations we will show that this approach is justified (Section 3.3).

The purity of the helium was 99.996% (Messer). Traces of oxygen were removed with Oxisorb cartridges (Messer). Double distilled water was introduced by a second gas

saturation system. The purity of the aromatic reactants was checked by gas-chromatographic analysis (50 m capillary column and flame ionization detector). 1,3,5-TMB (Fluka, 99+) had a purity of 99.4% and contained 0.6% of 1,2,4-TMB. 1,2,4-TMB (Fluka, 99+) was found to be 98.9% pure and contained 0.6% of 2-ethyltoluene, 0.3% of 1,2,3-TMB and 0.2% of 1,3,5-TMB. 1,2,3-TMB was available only with technical grade specification (Aldrich, >90%) but was found to have a purity of 94.2% and to contain 2.3% of 1,2,4-TMB, 0.2% of 1,3,5-TMB and 3.3% of ethyl-dimethylbenzenes.

3 Results and discussion

3.1 Reaction models and analytical solutions

3.1.1 Formation of one adduct species – model-1. The basic kinetic model of adduct formation and the corresponding analytical solutions will be summarized here briefly for direct comparison with the extended approach. Moreover, we derived more general expressions than previously that may also be applied at different boundary conditions and for other chemical systems (Section S1, ESI†).

OH radicals are assumed to react with aromatic compounds under reversible formation of a single adduct (add):

$$\text{OH} + \text{aromatic} \rightleftharpoons \text{add} \ (k_{1a}, k_{-1a}) \quad \text{(R1a /–1a)}$$
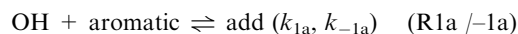
The corresponding first- and second-order rate constants are defined in brackets. Other, irreversible reactions are also possible, in particular abstraction reactions for substituted aromatics at higher temperatures:

$$\text{OH} + \text{aromatic} \rightarrow \text{products} \ (k_{1b}) \quad \text{(R1b)}$$
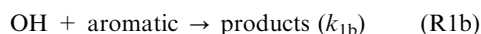
OH and the adduct may also react with impurities, by wall loss, or vanish from the observation zone by diffusional spread. These processes are usually minor, independent of the aromatics concentration and accounted for by two further hypothetical reactions:

$$\text{OH} \rightarrow \text{products} \ (k_2) \quad \text{(R2)}$$

$$\text{add} \rightarrow \text{products} \ (k_3) \quad \text{(R3)}$$
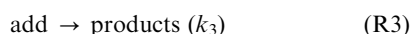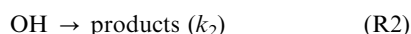
Any decomposition of the adduct to products other than OH will also increase k_3. Moreover, k_3 may be increased deliberately by addition of reactants such as O_2, NO, or NO_2 to study the kinetics of the corresponding adduct reactions.[6,7]

The analytical solution of the system of differential equations corresponding to reactions (R1a /–1a), (R1b), (R2), and (R3) leads to biexponential decay curves for OH:[4]

$$[\text{OH}] = C_1 \exp(-t/\tau_1) + C_2 \exp(-t/\tau_2) \quad (1)$$

$$\tau_{1,2}^{-1} = \frac{a+d}{2} \pm \sqrt{\left(\frac{a-d}{2}\right)^2 + bc} \quad (2)$$

The coefficients a, b, c and d are related to the rate constants by the following equations:

$$a = (k_{1a} + k_{1b})[\text{aromatic}] + k_2 \quad (3)$$

$$b = k_{-1a} \quad (4)$$

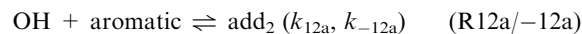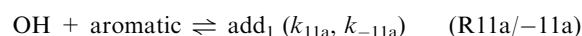$$c = k_{1a}[\text{aromatic}] \quad (5)$$

$$d = k_{-1a} + k_3 \quad (6)$$

Moreover, under experimental conditions with $[\text{add}]_0 = 0$, *i.e.* pulsed formation of OH at $t = 0$, the following expression can be derived for the ratio of the amplitudes C_1 and C_2 of the two exponentials at $t = 0$ (Section S1, ESI†):
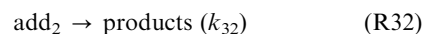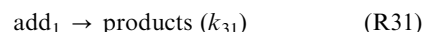
$$C_{1/2} = C_1/C_2 = \frac{\tau_1^{-1} - d}{d - \tau_2^{-1}} \quad (7)$$

Under pseudo-first-order conditions, *i.e.* independent of the OH starting concentration, a biexponential OH decay curve is therefore described by three curve parameters: $C_{1/2}$, τ_1^{-1} and τ_2^{-1}. These curve parameters can be calculated from the three coefficients a, d and the product bc related to the rate constants of the reactions involved, and *vice versa*. However, the product bc cannot be separated, *i.e.* the system is generally under-determined. A more general solution also covering the case where $[\text{add}]_0 \neq 0$ is given in the ESI† (Section S1).

3.1.2 Formation of two adduct species – model-2. With two adducts the chemical reaction scheme can be described as follows:

$$\text{OH} + \text{aromatic} \rightleftharpoons \text{add}_1 \ (k_{11a}, k_{-11a}) \quad \text{(R11a/–11a)}$$

$$\text{OH} + \text{aromatic} \rightleftharpoons \text{add}_2 \ (k_{12a}, k_{-12a}) \quad \text{(R12a/–12a)}$$

Irreversible losses of OH and the adducts are treated similarly as in the case of one adduct, *i.e.* by reactions (R1b) and (R2), and the following two reactions:

$$\text{add}_1 \rightarrow \text{products} \ (k_{31}) \quad \text{(R31)}$$

$$\text{add}_2 \rightarrow \text{products} \ (k_{32}) \quad \text{(R32)}$$

Solution of the corresponding system of differential equations now yields triexponential decay curves for OH:

$$[\text{OH}] = C_1 \exp(-t/\tau_1) + C_2 \exp(-t/\tau_2) + C_3 \exp(-t/\tau_3) \quad (8)$$

The expressions for the decay rate coefficients τ_{1-3}^{-1} are more complicated, but can basically be expressed as a function of three parameters r, s, and u (Section S2, ESI†):

$$r = -a - d - g \quad (9)$$

$$s = ad + dg + ag - bc - ef \quad (10)$$

$$u = bcg + efd - adg \quad (11)$$

The coefficients a, b, c, d, e and f are again related to the rate constants:

$$a = (k_{11a} + k_{12a} + k_{1b})[\text{aromatic}] + k_2 \quad (12)$$

$$b = k_{-11a} \quad (13)$$

$$c = k_{11a}[\text{aromatic}] \quad (14)$$

$$d = k_{-11a} + k_{31} \quad (15)$$

$$e = k_{-12a} \quad (16)$$

$$f = k_{12a}[\text{aromatic}] \quad (17)$$

$$g = k_{-12a} + k_{32} \quad (18)$$

With $[\mathrm{add}_1]_0 = 0$ and $[\mathrm{add}_2]_0 = 0$, equations were derived for the ratios of the initial values $C_{1/2}$ and $C_{3/2}$ (Section S2, ESI†).

$$C_{1/2} = C_1/C_2 = \frac{(d - \tau_1^{-1})(g - \tau_1^{-1})(\tau_3^{-1} - \tau_2^{-1})}{(d - \tau_2^{-1})(g - \tau_2^{-1})(\tau_1^{-1} - \tau_3^{-1})} \quad (19)$$

$$C_{3/2} = C_3/C_2 = \frac{(d - \tau_3^{-1})(g - \tau_3^{-1})(\tau_2^{-1} - \tau_1^{-1})}{(d - \tau_2^{-1})(g - \tau_2^{-1})(\tau_1^{-1} - \tau_3^{-1})} \quad (20)$$

Triexponential OH decay curves are therefore characterized by five curve parameters: $C_{1/2}$, $C_{3/2}$, τ_1^{-1}, τ_2^{-1} and τ_3^{-1}. These curve parameters can be calculated from the five coefficients a, d, g, and the products bc and ef related to the rate constants of the reactions involved, and *vice versa*. The products bc and ef cannot be separated, *i.e.* the system is again under-determined. Moreover, as is evident from eqn (19) and (20), the variables d and g are exchangeable. Thus we arbitrarily chose $d > g$ to distinguish between add_1 and add_2. In the ESI† (Section S2) we give more general expressions for the case $[\mathrm{add}_1]_0 \neq 0$ and/or $[\mathrm{add}_2]_0 \neq 0$ which may be useful for other applications. To our knowledge these analytical solutions have not been published before. Preliminary results based on this reaction model were presented during a Workshop on Atmospheric Chemistry, University of Bayreuth, 24–26 February, 2010.

3.1.3 Formation of two adduct species with isomerization – model-3. The possibility that has not been considered so far is that the adduct isomers convert into each other by an isomerization reaction:

$$\mathrm{add}_1 \rightleftharpoons \mathrm{add}_2 \ (k_{12}, k_{21}) \quad (\text{R12/R21})$$
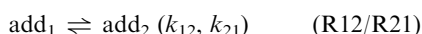
Of course that further complicates the analytical solution, but the OH decay curves remain triexponential and only the parameters s and u in eqn (10) and (11) change:

$$s = ad + dg + ag - bc - ef - hi \quad (21)$$

$$u = bcg + efd - adg + eic + hia + fbh \quad (22)$$

The new coefficients i and h are related to the isomerization reaction rate constants:

$$i = k_{12} \quad \text{and} \quad h = k_{21} \quad (23)$$

Obviously the product hi is a further fit parameter that has to be determined here. In addition the "mixed" products eic and fbh seem to complicate things further. However, the rate constants involved in this extended mechanism were assumed to obey an additional relation that comes from detailed balancing considerations:[21]

$$\frac{k_{12a}}{k_{-12a}} \frac{k_{21}}{k_{12}} \frac{k_{-11a}}{k_{11a}} = 1 \quad (24)$$

In terms of the above parameters that means:

$$fbh = eic = \sqrt{bc \, ef \, hi} \quad (25)$$

Setting $[\mathrm{add}_1]_0 = 0$ and $[\mathrm{add}_2]_0 = 0$ ratios of initial values $C_{1/2}$ and $C_{3/2}$ were again obtained (Section S3, ESI†). Also the triexponential OH decay curves of model-3 are described by five curve parameters: $C_{1/2}$, $C_{3/2}$, τ_1^{-1}, τ_2^{-1} and τ_3^{-1} but in this case they have to be calculated from six coefficients: a, d, g, and the products bc, ef and hi related to the reaction rate constants.

The products bc, ef and hi cannot be separated, as before. Moreover, the fact that six coefficients determine five curve parameters already implies that there is no unique relationship between these quantities.

3.2 Data analysis

The simplest approach to evaluate OH decay curves is to fit the curve parameters for each curve separately using a non-linear least-squares fitting procedure. For a biexponential decay these parameters are $C_{1/2}$, τ_1^{-1} and τ_2^{-1}. For a triexponential decay $C_{1/2}$, $C_{3/2}$, τ_1^{-1}, τ_2^{-1}, and τ_3^{-1} must be determined. Additional parameters to fully describe an experimental curve are the starting signal, *i.e.* a count rate proportional to $[\mathrm{OH}]_0$, and the background signal. That gives a total of five or seven fit parameters for each curve, dependent on the chemical model.

Taking a biexponential decay curve as an example, the three fitted curve parameters can be converted to the coefficients a, d and bc (Section S1, ESI†). OH decay curves were measured at various aromatics concentrations. Plainly, a linear regression of a as a function of [aromatic] would then give a slope and an intercept corresponding to the sum of rate constants $k_{1a} + k_{1b}$ and k_2, respectively (eqn (3)). The linearity of the dependence of a on [aromatic] as well as the constancy of d for a given temperature can serve as a test for the validity of the kinetic model. Moreover, to isolate b and c, it can be assumed that for example in the case of benzene $k_{1b} = 0$ as a good approximation, *i.e.* $c = a - k_2$ (no reaction except addition). For methyl-substituted aromatics k_{1b} can be estimated from an extrapolation of high-temperature abstraction rate constants,[22] *i.e.* $c = a - k_{1b}[\mathrm{aromatic}] - k_2$ (eqn (3) and (5)).

However, fitting curve parameters of each decay curve separately is not the best method of data analysis. The range of useful experimental conditions can be extended by an approach where several decay curves obtained at different reactant concentrations are fitted simultaneously. The advantage is that also curves where a single fit would be critical because the reciprocal lifetimes approach each other or the amplitude ratio $C_{1/2}$ is getting too small or too great, are still useful if evaluated together with other curves. Moreover, the procedures described above consist of two steps to finally derive rate constants. On the other hand, the rate constants can be obtained directly as parameters from a simultaneous fit to all decay curves measured at constant temperature and pressure. In these fits the experimental errors of all data points and their influence on the rate constants are taken into account more directly and consistently. This approach was used successfully and was described in previous work[6,7] but was so far confined to the reaction model resulting in biexponential decay curves.

In the present study isothermal arrays of decay curves were fitted simultaneously using the programming language IDL by Research Systems Inc. For model-1 (biexponential curves), a fit-function was defined that – upon input of m experimental reactant concentrations, and arrays of measurement times and interval widths – calculates the m decay curves from $4 + 2m$ fit parameters (Section S4, ESI†). The parameters are (1) k_2, (2) $k_{1a} + k_{1b} = (a - k_2)/[\mathrm{aromatic}]$, (3) $k_{1a}k_{-1a} = bc/[\mathrm{aromatic}]$, and (4) $k_{-1a} + k_3 = d$, as well as the m initial count rates S_0

This journal is © the Owner Societies 2012

Phys. Chem. Chem. Phys., 2012, **14**, 13933–13948 | 13937

and backgrounds S_B for each curve. Reasonable starting values for S_0 and S_B were obtained from pre-fits to the individual curves. From the starting values of the first four parameters and the aromatics concentrations the coefficients a, bc, d and the resulting $C_{1/2}$ and $\tau_{1,2}^{-1}$ were calculated for each curve. Optimization of all fit parameters by comparison with the experimental curves was then accomplished by a non-linear Levenberg–Marquardt fitting procedure.[23] In the fits each data point was weighted according to Poisson counting statistics, *i.e.* with a ratio n/N where n is the number of originally accumulated decays and N is the number of counted photons (Section S4, ESI†).

The procedure to fit arrays of triexponential decay curves was technically similar but the number of optimized parameters was greater: $6 + 2m$. The first six parameters for model-2 are (1) k_2, (2) $k_{11a} + k_{12a} + k_{1b} = (a - k_2)/$[aromatic], (3) $k_{11a}k_{-11a} = bc/$[aromatic], (4) $k_{12a}k_{-12a} = ef/$[aromatic], (5) $k_{-11a} + k_{31} = d$, and (6) $k_{-12a} + k_{32} = g$. For model-3 we also fitted six parameters: (1) k_2, (2) $k_{11a} + k_{12a} + k_{1b} = (a - k_2)/$[aromatic], (3) $k_{11a}k_{-11a} = bc/$[aromatic], (4) $k_{12}k_{21} = hi$, (5) $k_{-11a} + k_{12} + k_{31} = d$, and (6) $k_{21} + k_{32} = g$. The parameter $ef/$[aromatic] was held fixed at a very small value, *i.e.* $k_{12a}k_{-12a} \approx 0$, to simulate a case of add$_2$ formation only by isomerization. A full fit adjusting all seven parameters of model-3 was not performed as will be explained below.

No attempt was made to individually analyze single decay curves, neither biexponential, nor triexponential because there is no reason for such a step backward. Considering groups of decay curves obtained at the same temperature is the optimum procedure to identify and quantify any differences between the various model approaches. Whether or not the applied chemical models are consistent with the experimental data can be assessed from the fitted sum of weighted squared residuals χ^2 divided by the degrees of freedom. The degrees of freedom (DOF) are the number of data points minus the number of fitted parameters, *i.e.* $59m - 4$ for a model-1 fit and $59m - 6$ for a model-2 or model-3 fit, respectively. Deviations of $\chi^2/$DOF towards values much greater than unity indicate that the applied fit function is not suitable or that experimental errors were underestimated. On the other hand, values well below unity in any case indicate an overestimation of experimental errors. Thus a thorough assessment of experimental errors in the fitting procedure is crucial for the judgement of fit quality and the applicability of a fit function. Based on simulated experimental data for model-1 and model-2 including experimental random noise according to Poisson statistics we confirmed that the fit routines on average return $\chi^2/$DOF = 1.00 with a standard deviation of about 0.08 (Section S5.1, ESI†). For experimental data somewhat greater values are expected because a mean value $\chi^2/$DOF = 1.00 is a theoretical limit in the case of accurately known experimental errors and data that without these errors are in perfect agreement with the underlying model (as in the simulations). Typically there are additional, unaccounted sources of errors that lead to somewhat greater values.

Error limits of the fitted parameters were estimated as recently introduced in similar applications of the least-squares fitting procedure.[24] Successively, the four (model-1) and six (model-2, model-3) parameters were stepwise increased or decreased starting with the optimum values and held fixed in the fits until the ratio $\chi^2/$DOF increased by a predefined factor. This factor ranged between 1.02 and 1.03 dependent on DOF and was taken from a parametrization of the χ^2-distribution for a probability of 0.68. All other parameters were allowed to adjust freely during these fits, *i.e.* the resulting ranges reflect error limits that cover the mutual dependence of the fit parameters. The original idea was that this procedure results in estimated 1σ error limits. However, based on the simulated experimental data it turned out that these errors are greater by about a factor of three compared to the standard deviations of the parameters resulting from the simulations (Section S5.3, ESI†). The error estimates are therefore rather conservative but nevertheless they cannot account for systematic deviations that arise when the applied chemical model is incorrect.

3.3 Comparison of model-1 and model-2 results

Fig. 1 shows examples of normalized OH decay curves obtained in the presence of various 1,3,5-TMB concentrations at 324 K (experiment 10, Table 1). Only four curves (out of the total array of seven that were fitted simultaneously) are shown for clarity. As mentioned before, actual measurement times extended up to 5 s for an accurate determination of the background that was subtracted in the displayed plots but considered in the error bars. The unequal spacing of the data points is caused by the data compression. The full lines are fits according to model-1 and model-2. Because fitted background levels and starting values were slightly different for the two models, also the data points in Fig. 1 differ slightly. In this example, the triexponential model-2 clearly describes the data better than the biexponential model-1 as will be discussed in more detail below.

Fitted parameters of model-1 and model-2 for all 1,3,5-TMB experiments are listed in Tables 1 and 2 and plotted in Fig. 2 in semi-logarithmic representations as a function of reciprocal temperatures (Arrhenius plots). In addition, $\chi^2/$DOF is shown on a linear scale. For experiments 1–3 at temperatures below 290 K, fits using model-2 either failed to converge or became biexponential, *i.e.* identical to model-1. However, towards higher temperatures the two models led to significantly different results. Moreover, while the quality of the fits of model-1 decreased with rising temperature, that of model-2 remained in an acceptable range with $\chi^2/$DOF $\leq$ 1.5. This is clear evidence that model-2 is in better accordance with the experimental data than model-1, at least at higher temperatures. Obviously two species with significantly different properties are formed in the reaction of OH with 1,3,5-TMB. Although no structural information was obtained here, we assume that these species are *ortho-* and *ipso-*type adducts.

Independent of the applied model, no dependence on total pressure was found at 380 or 750 hPa of He. Thus, all reactions were at their high pressure limits – in accordance with previous work also on other aromatics.[6,25,26] The OH background loss rate constant k_2 decreased significantly with increasing temperature and showed little dependence on total pressure. This behaviour was confirmed by measurements in the absence of added aromatics. The nature of the background
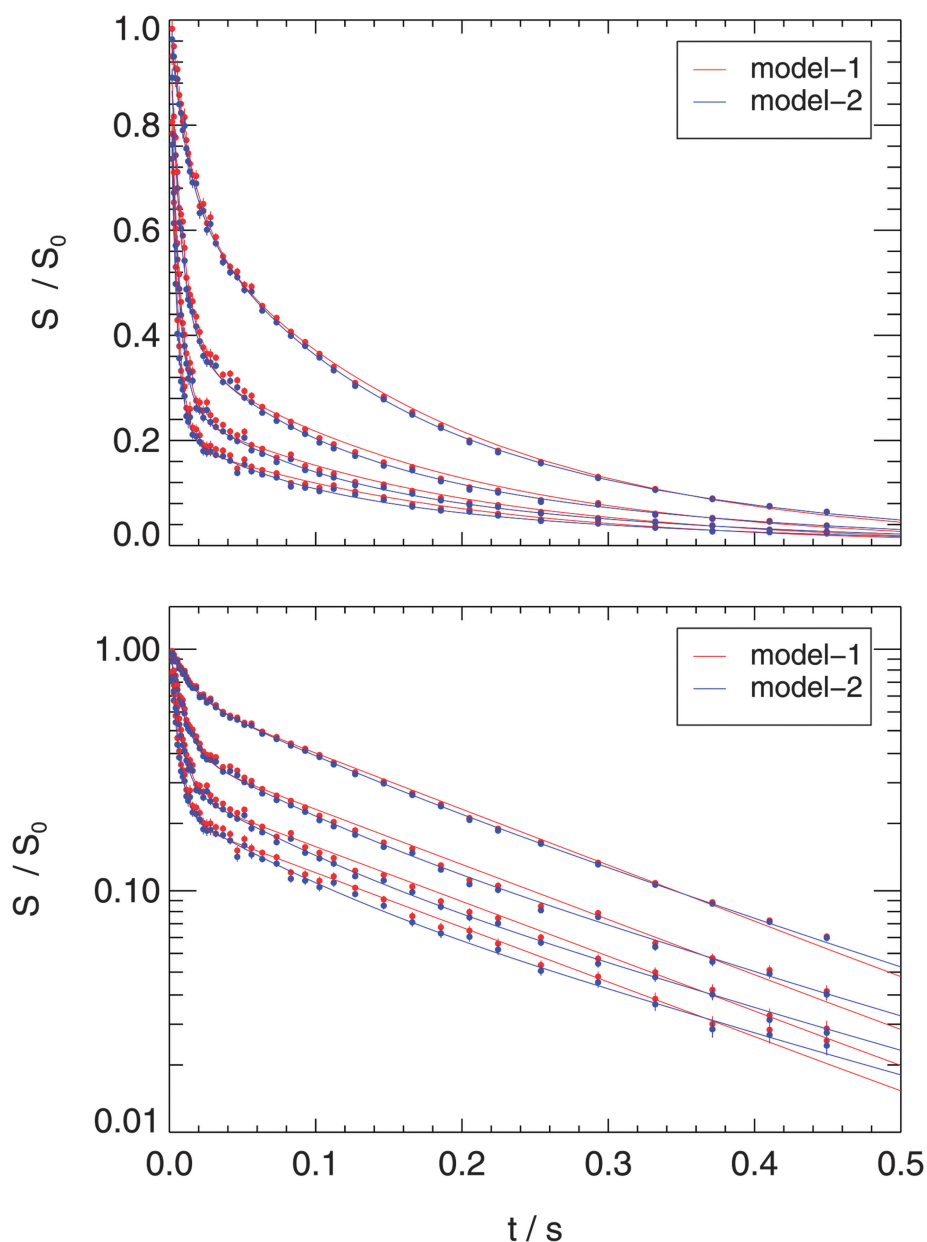
Fig. 1 Examples of OH decay curves in linear and semi-logarithmic representations. Four from a total of seven decay curves of experiment 10 with 1,3,5-TMB at 324 K are shown. 1,3,5-TMB concentrations increase from top to bottom (in units 10^{12} cm^{-3}: 0.48, 1.42, 2.39, 3.31). Full lines are fits to all curves simultaneously using model-1 (red) and model-2 (blue). Data points were calculated from photon counts N divided by interval widths and assigned to the middle of the interval. Fitted background levels were subtracted and the data were then normalized by the fitted starting count rates for better comparability.

loss is unknown but is probably dominated by impurities because diffusional losses would increase at decreasing pressure and increasing temperature. However, the influence of k_2 on the other results is minor and the fitted values were very similar for both models.

Based on numerical simulations we confirmed that neither radical–radical reactions nor diffusion processes can lead to deviations that would pretend a different reaction model (Sections S5.1 and S5.2, ESI†). The simulation results are supported by a series of experiments with 1,2,4-TMB where the flash-energy was lowered by a factor of two with no noticeable effect on fitted rate constants (Section S6, ESI†) and by the independence of total pressure.

3.3.1 OH + TMB rate constants. The second-order rate constants k_{OH} of OH + 1,3,5-TMB were obtained directly as fit parameters and assigned to the sum $k_{1a} + k_{1b}$ for model-1 and $k_{11a} + k_{12a} + k_{1b}$ for model-2, respectively. The rate constants obtained here for model-1 are identical to those determined previously,[10] confirming that the different software tools worked consistently. At temperatures below about 300 K both models gave the same rate constants. Moreover, for both models k_{OH} decreased with increasing temperature. However, towards higher temperatures the rate constants of model-1 show a stronger decrease. Because of the poorer fit quality we consider this strong decrease as an artefact of the data analysis of model-1 while the results of model-2 are presumed to be correct.

Table 2 Triexponential model-2 fit results and estimated error limits from simultaneous fits to m decay curves at different 1,3,5-TMB concentrations (see Table 1 for m and experimental conditions)

#	k_2/s^{-1}	$k_{11a} + k_{12a} + k_{1b}/$ $10^{-11}\text{ cm}^3\text{ s}^{-1}$	$k_{11a}k_{-11a}/$ $10^{-10}\text{ cm}^3\text{ s}^{-2}$	$k_{12a}k_{-12a}/$ $10^{-10}\text{ cm}^3\text{ s}^{-2}$	$k_{-11a} + k_{31}/\text{s}^{-1}$	$k_{-12a} + k_{32}/\text{s}^{-1}$	DOF	$\chi^2/$DOF
4	9.7 ± 3.9	$6.22 \pm {}^{0.32}_{0.30}$	$1.85 \pm {}^{0.73}_{0.79}$	$0.67 \pm {}^{0.61}_{0.48}$	$15.9 \pm {}^{19}_{7.1}$	$3.3 \pm {}^{1.8}_{2.0}$	348	0.95
5	14.7 ± 2.5	$5.91 \pm {}^{0.24}_{0.23}$	$2.35 \pm {}^{0.50}_{0.74}$	$0.83 \pm {}^{0.77}_{0.57}$	$12.3 \pm {}^{8.6}_{3.7}$	$3.7 \pm {}^{1.3}_{1.5}$	407	1.32
6	9.8 ± 0.9	$5.98 \pm {}^{0.21}_{0.18}$	$2.67 \pm {}^{0.43}_{0.54}$	$0.82 \pm {}^{0.59}_{0.48}$	$14.1 \pm {}^{6.8}_{3.7}$	$4.0 \pm {}^{1.1}_{1.3}$	407	1.10
7	10.1 ± 1.5	$5.82 \pm {}^{0.21}_{0.20}$	$4.52 \pm {}^{0.47}_{0.75}$	$0.62 \pm {}^{0.90}_{0.41}$	$14.7 \pm {}^{4.6}_{2.4}$	$4.5 \pm {}^{1.9}_{1.7}$	407	1.28
8	8.8 ± 0.6	$5.46 \pm {}^{0.22}_{0.19}$	$10.7 \pm {}^{0.83}_{0.73}$	$0.47 \pm {}^{0.43}_{0.23}$	$27.3 \pm {}^{3.0}_{2.2}$	$6.4 \pm {}^{1.9}_{1.6}$	407	1.27
9	7.8 ± 0.4	$5.71 \pm {}^{0.35}_{0.31}$	$17.9 \pm {}^{2.1}_{1.8}$	$0.32 \pm {}^{0.39}_{0.17}$	$39.6 \pm {}^{4.2}_{3.2}$	$7.0 \pm {}^{3.0}_{2.1}$	407	1.57
10	5.4 ± 0.3	$5.46 \pm {}^{0.51}_{0.45}$	$27.0 \pm {}^{3.7}_{3.9}$	$0.33 \pm {}^{0.41}_{0.18}$	$59.6 \pm {}^{7.3}_{5.7}$	$9.0 \pm {}^{3.8}_{2.8}$	407	1.31
11	4.9 ± 0.2	$5.00 \pm {}^{0.89}_{0.74}$	$54.9 \pm {}^{17.3}_{12.8}$	$0.26 \pm {}^{0.32}_{0.14}$	$125 \pm {}^{17}_{14}$	$13.2 \pm {}^{5.7}_{4.1}$	407	1.38
12	4.9 ± 0.2	$4.81 \pm {}^{0.98}_{0.77}$	$50.0 \pm {}^{19.5}_{12.8}$	$0.12 \pm {}^{0.60}_{0.10}$	$117 \pm {}^{23}_{15}$	$10.8 \pm {}^{13}_{6.5}$	407	1.27
13	5.1 ± 0.1	$5.43 \pm {}^{1.07}_{0.87}$	$99.2 \pm {}^{36.0}_{24.7}$	$0.38 \pm {}^{0.58}_{0.24}$	$205 \pm {}^{30}_{24}$	$23.1 \pm {}^{10}_{8.0}$	407	1.54
14	5.1 ± 0.2	$5.37 \pm {}^{1.35}_{1.08}$	$107 \pm {}^{46}_{33}$	$0.18 \pm {}^{0.22}_{0.09}$	$221 \pm {}^{34}_{29}$	$14.3 \pm {}^{6.6}_{4.7}$	407	1.79

In contrast to those of model-1, the rate constants of model-2 can be described empirically by a straight Arrhenius dependence $k_{\text{OH}} = A_1 \exp(-B_1/T)$ as indicated by the full blue line in the upper panel of Fig. 2. Only a minor difference was obtained using a combination of data from model-2 above 290 K and of model-1 below 290 K (dashed blue line in Fig. 2). Because the latter combination is covering a wider temperature range we prefer the corresponding Arrhenius parameters that are given in Table 3. The simpler temperature dependence resulting from model-2 is in agreement with literature data by Aschmann et al.[27] obtained with a relative rate method in a similar range of temperatures as indicated by the dashed black line in Fig. 2. Although the absolute values are somewhat smaller compared with the results of this work, the general temperature dependence is similar and confirms the advantage of model-2. Table 3 also lists other room temperature rate constants of OH + 1,3,5-TMB from the literature that are in good agreement with that of this work.

The fit results obtained with 1,2,3-TMB and 1,2,4-TMB will not be discussed here in detail because the model-2 approach does not strictly apply to these compounds. Nevertheless, by switching from model-1 to model-2 we obtained qualitatively similar results, namely a significant improvement of fit qualities towards greater temperatures and a weaker decrease of k_{OH} with temperature. Fit results and plots can be found in the ESI† (Section S6). The improvement of the fit quality can be rationalized by the fact that the four and six possible isomers for 1,2,3-TMB and 1,2,4-TMB fall into two groups of ortho- and ipso-type adducts with presumably similar properties within the groups. Consequently, we assume that also the k_{OH} are more reliable than those obtained with model-1 that were published previously.[10] As for 1,3,5-TMB, the k_{OH} can now be described by straight Arrhenius expressions in good approximation. The corresponding parameters, together with a comparison of available room temperature rate constants from the literature are given in Table 3.

3.3.2 Adduct loss rate constants. In contrast to the k_{OH}, the fitted first-order rate constants of adduct loss of 1,3,5-TMB, k_{add}, increased with temperature and levelled out to small values at low temperatures as shown in the second panel of Fig. 2. These rate constants correspond to the sums $k_{-1a} + k_3$ for model-1, as well as $k_{-11a} + k_{31}$ (add$_1$) and $k_{-12a} + k_{32}$ (add$_2$)

for model-2. In fact, with model-2 two strongly different k_{add} were obtained while that for model-1 expectedly lies in between these extremes, albeit at the expense of a poorer fit quality. Again we conclude that model-2 may describe the actual properties of two adduct isomers while the result of model-1 is an inadequate compromise. The full lines in Fig. 2 show that the temperature dependencies of all three quantities can be described by modified Arrhenius expressions $k_{\text{add}} = A_2 \exp(-B_2/T) + C$ that allowed for a constant, temperature independent contribution of background loss reactions. Unlike the k_2, that could be determined independently and separated from k_{OH}, the adduct background loss cannot be measured directly. Therefore we assumed temperature independent contributions (C) of k_3, k_{31} and k_{32} while the k_{-1a}, k_{-11a} and k_{-12a} were found to increase exponentially with temperature. The three different A_2, B_2 and C are listed in Table 4. The A_2 vary over many orders of magnitude. Because of the narrow range of temperatures investigated here, this parameter is extremely uncertain. On the other hand, the B_2 and C are comparable and lie in a range 5000–10 000 K and 1–8 s^{-1}, respectively. Uncertainties for these parameters were estimated by fitting maximum and minimum values of the data in Tables 1 and 2. Within these limits the B_2 of the two adduct isomers of model-2 are significantly different but unexpectedly the smaller k_{add} of add$_2$ corresponds to a smaller B_2 because of the extremely small A_2. Despite the uncertainties caused by the narrow T-range, the A_2 of add$_2$ seems unrealistically low because preexponential factors usually range around 10^{11}–10^{16} s^{-1} for unimolecular reactions.[28]

Previous studies on benzene,[6,13] toluene[6,13] and p-xylene[14] gave very similar results for B_2 and C in a range 7700–8800 K and 2.5–5.5 s^{-1}, respectively (Table 4). This matches very well with the result obtained here for 1,3,5-TMB with model-1 and is also in reasonable agreement with the properties of add$_1$ of model-2. For example, taking a typical experimental temperature of 320 K, the values for k_{add} range between 20 and 30 s^{-1} for benzene, toluene, p-xylene and 1,3,5-TMB, all based on model-1. For model-2 this rate constant only slightly increases to 36 s^{-1} for add$_1$ but drops more strongly to 6 s^{-1} for add$_2$. Because a single, high-temperature study on hexamethylbenzene (HMB)[29] revealed the existence of a very stable ipso-adduct with an extrapolated dissociation rate constant of 0.6 s^{-1} at 320 K, we therefore tentatively identify add$_2$ as the ipso-isomer and add$_1$

13940 | Phys. Chem. Chem. Phys., 2012, **14**, 13933–13948
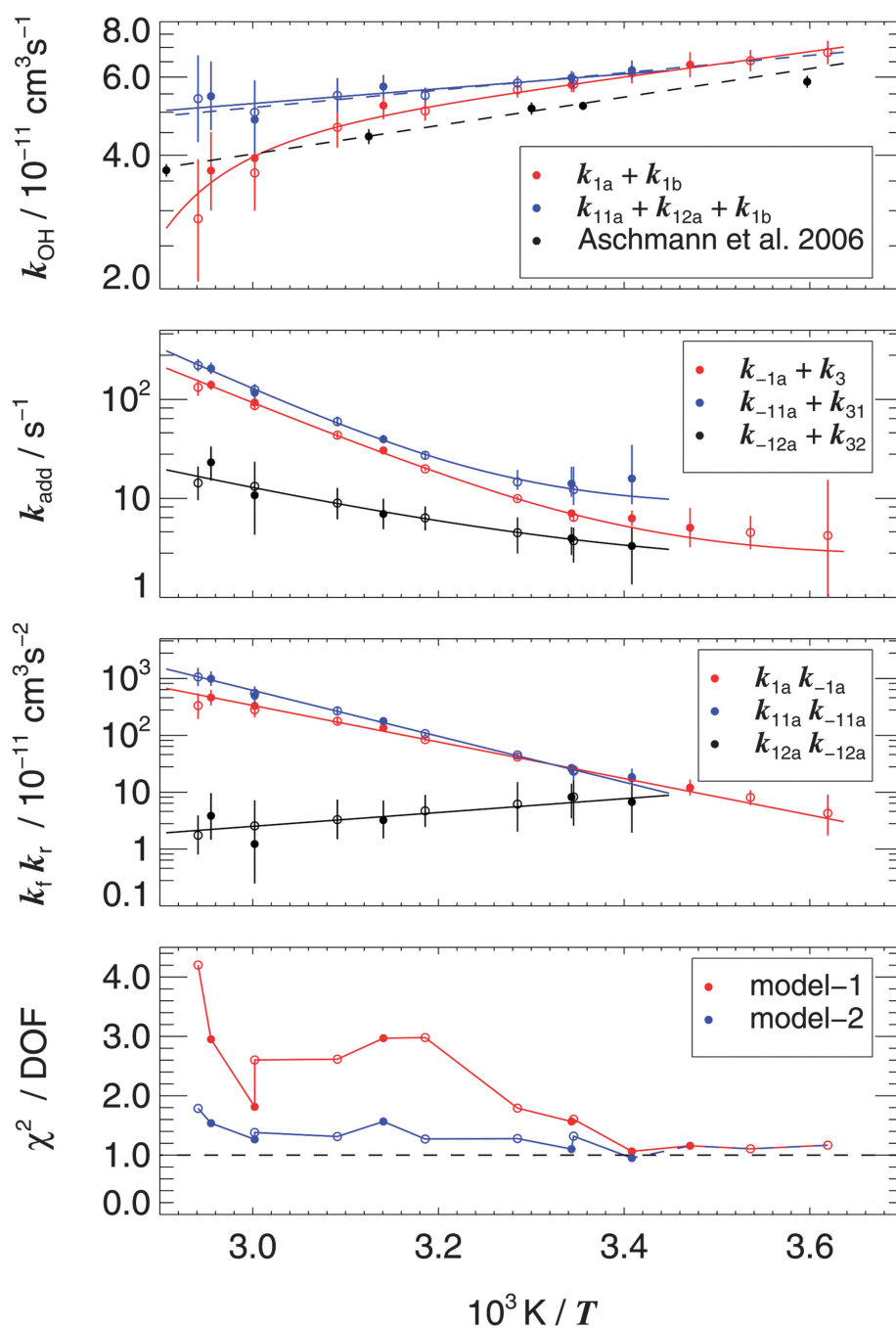
This journal is © the Owner Societies 2012

Fig. 2 Rate constant related fit parameters and fit qualities χ^2/DOF for 1,3,5-TMB using model-1 (red) and model-2 (black, blue). Open symbols refer to measurements at 380 mbar and filled symbols at 750 mbar. Full lines in the upper three panels correspond to fitted Arrhenius expressions except for the red line in the first panel that shows a previous parametrization from the literature.[10] The dashed blue line in the first panel is an Arrhenius fit using model-2 data above 290 K together with model-1 data below 290 K. Black points and the dashed black line show a temperature dependence from the literature.[27] In the second panel temperature independent contributions of background loss rate constants were assumed. The dashed blue lines on top of the red line in the fourth panel indicate that models converged towards low temperatures. The dashed black line shows a theoretical optimum.

as the *ortho*-isomer. On the other hand, the B_2 obtained for the HMB adduct was much greater (10 500 K)[29] and comparable with that of add$_1$ of this work. Clearly more information is necessary to identify the adduct isomers.

3.3.3 Products of forward and backward rate constants, isomer yields and heats of formation.

The products of the forward and reverse reactions $k_f k_r$ are further direct fit parameters that correspond to $k_{1a}k_{-1a}$ for model-1, as well as $k_{11a}k_{-11a}$ and $k_{12a}k_{-12a}$ for model-2. The temperature dependencies of these quantities could also be described by simple Arrhenius expressions $k_f k_r = A_3 \exp(-B_3/T)$ in good approximation, as indicated by the full lines in the third panel of Fig. 2. The parameters A_3 and B_3 are listed in Table 5. For the A_3 the same applies as for the A_2 in the last section: these quantities are extremely uncertain because of the confined

Table 3 Room temperature rate constants k_{OH} of OH + TMB reactions and parameters A_1 and B_1 from fitted Arrhenius expressions $k_{OH} = A_1 \exp(-B_1/T)$ compared with literature data. The data of this work apply for a temperature range 275–340 K using a combination of results of model-1 at $T < 290$ K and of model-2 at $T > 290$ K (see text). The estimated 10% systematic uncertainty of aromatics concentrations is not included in the error limits. The same applies to the results of Aschmann et al.[27] where an estimated 10% uncertainty of the reference compound rate constant was not included

Reactant	$k_{OH}{}^a/10^{-11}$ cm^3 s^{-1}	$A_1/10^{-12}$ cm^3 s^{-1}	$B_1/10^3$ K	Ref.
1,3,5-TMB	4.72 ± 0.48	—	—	Hansen et al.[25]
	6.24 ± 0.75	—	—	Perry et al.[26]
	5.75 ± 0.30	—	—	Atkinson et al.[38]
	5.73 ± 0.53	—	—	Kramp and Paulson[39]
	5.91 ± 0.11	—	—	Aschmann et al.[40]
	5.17 ± 0.11	4.4	0.74 ± 0.18	Aschmann et al.[27]
	5.95 ± 0.20	13.2	-0.45 ± 0.05^b	This work
1,2,3-TMB	2.64 ± 0.26			Hansen et al.[25]
	3.33 ± 0.45			Perry et al.[26]
	3.27 ± 0.19			Atkinson et al.[38]
	2.88 ± 0.10	3.61	-0.62 ± 0.08^b	This work
1,2,4-TMB	3.35 ± 0.34			Hansen et al.[25]
	4.00 ± 0.45			Perry et al.[26]
	3.25 ± 0.11			Atkinson et al.[38]
	3.05 ± 0.20	2.73	-0.73 ± 0.07^b	This work

^{a} 298 $\pm$ 2 K. ^{b} Error limits from fits to maximum and minimum k_{OH}.

Table 5 Parameters A_3 and B_3 from fitted Arrhenius expressions $k_f k_r = A_3 \exp(-B_3/T)$ to products of forward and reverse rate constants for 1,3,5-TMB. For model-1: $k_f k_r = k_{1a} k_{-1a}$. For model-2: $k_f k_r = k_{11a} k_{-11a}$ (add$_1$) and $k_f k_r = k_{12a} k_{-12a}$ (add$_2$). For model-3: $k_f k_r = k_{11a} k_{-11a}$ (add$_1$), $k_f k_r = 0$ (add$_2$) and $k_f k_r = k_{12} k_{21}$ (add$_1$ $\rightleftharpoons$ add$_2$) (pure isomerization limit)

$k_f k_r$	A_3/cm^3 s^{-2}	$B_3/10^3$ K^a
Mod-1	14.7	7.4 ± 0.2
Mod-2, add$_1$	8.1×10^3	9.3 ± 0.2
Mod-2, add$_2$	5.7×10^{-15}	-2.8 ± 0.3
Mod-3, add$_1$	3.3×10^2	8.3 ± 0.2
	A_3/s^{-2}	
Mod-3, add$_1$ $\rightleftharpoons$ add$_2$	2.4×10^8	5.1 ± 0.3

^{a} Error limit estimated from fits to maximum and minimum $k_f k_r$.

The ratios k_f/k_{OH} then determine the adduct yields of the OH reaction.

It turned out that towards low temperatures when the denominators in eqn (27) were getting very small, the forward rate constant k_{11a} became greater than k_{OH} which is inconsistent with the OH reaction balance formulated in eqn (27). Instead of the C from Table 4 we therefore determined optimized values of k_3, k_{31} and k_{32} that were fitted based on eqn (26) and (27), and estimated values of k_{1b} from the literature. It was assumed that k_{1b} corresponds to the rate constant of the H-atom abstraction reaction from the substituent CH$_3$-groups.

Atkinson[22] derived an empirical expression for the rate constant per CH$_3$-group from high temperature data of the OH reaction with toluene and xylenes[26,30,31] that was extrapolated to the temperature range of this work and multiplied by three. However, these k_{1b} contribute no more than 5% to the overall k_{OH} and therefore have a minor influence. A similar extrapolation based on a different type of parameterisation of high temperature rate constants of toluene recommended by IUPAC[32] is leading to even smaller k_{1b} with a maximum contribution of 3% to k_{OH} in the temperature range considered here.

The optimized adduct background loss rate constants in terms of the OH reaction balance were $k_3 = 3.0$ s^{-1}, $k_{31} = 1.2$ s^{-1} and $k_{32} = 1.7$ s^{-1}. Only k_{31} is significantly smaller than the empirical parameter C in Table 4, but still reasonable

temperature range. Uncertainties of B_3 were again estimated by fitting maxima and minima of the data in Tables 1 and 2. The $k_f k_r$ exhibit an opposite temperature dependence for add$_1$ and add$_2$.

The rate constants of the forward reactions k_{1a}, k_{11a} and k_{12a} and thus the adduct yields can be determined from the $k_f k_r$ provided that the adduct background loss rate constants k_3, k_{31} and k_{32} are known. For model-1 k_{1a} is given by:

$$k_{1a} = \frac{k_f k_r}{k_r} = \frac{k_{1a} k_{-1a}}{k_{-1a}} = \frac{k_{1a} k_{-1a}}{k_{add} - k_3} = k_{OH} - k_{1b} \quad (26)$$

For model-2 a similar equation applies:

$$k_{11a} + k_{12a} = \frac{k_{11a} k_{-11a}}{k_{add_1} - k_{31}} + \frac{k_{12a} k_{-12a}}{k_{add_2} - k_{32}} = k_{OH} - k_{1b} \quad (27)$$

Table 4 Parameters A_2, B_2 and C from fitted Arrhenius expressions $k_{add} = A_2 \exp(-B_2/T) + C$ to adduct loss rate constants. For model-1: $k_{add} = k_{-1a} + k_3$. For model-2: $k_{add} = k_{-11a} + k_{31}$ (add$_1$) and $k_{add} = k_{-12a} + k_{32}$ (add$_2$). For model-3: $k_{add} = k_{-11a} + k_{12} + k_{31}$ (add$_1$) and $k_{add} = k_{21} + k_{32}$ (add$_2$) (pure isomerization limit). Literature data were obtained based on model-1

Reactant	k_{add}	A_2/s^{-1}	$B_2/10^3$ K	C/s^{-1}	Ref.
1,3,5-TMB	Mod-1	2.5×10^{13}	8.8 ± 0.7	2.6 ± 1.2	This work^a
	Mod-2, add$_1$	7.2×10^{14}	9.8 ± 1.1	8.3 ± 5.9	
	Mod-2, add$_2$	3.6×10^7	5.0 ± 1.0	1.9 ± 1.9	
	Mod-3, add$_1$	3.9×10^{14}	9.6 ± 0.9	6.1 ± 3.7	
	Mod-3, add$_2$	3.1×10^{10}	7.4 ± 3.2	5.2 ± 4.4	
Benzene	Mod-1^b	9.0×10^{12}	8.6 ± 0.2	3.3 ± 0.3	Knispel et al.[6]
		1.4×10^{12}	8.0 ± 0.5	3.0 ± 0.3	Koch[13]
Toluene	Mod-1	1.5×10^{12}	7.9 ± 0.2	4.8 ± 1.8	Knispel et al.[6]
		2.3×10^{12}	8.0 ± 0.8	5.0 ± 0.5	Koch[13]
p-Xylene	Mod-1	3.8×10^{12}	8.2 ± 0.3	4.8 ± 1.8	Knispel[14]
Hexamethyl-Benzene	Mod-1^b	1.0×10^{14}	10.5	4.0	von Buttlar et al.[29]

^{a} Error limit estimated from fits to maximum and minimum k_{add}. ^{b} Applies strictly for this compound.

13942 | Phys. Chem. Chem. Phys., 2012, **14**, 13933–13948

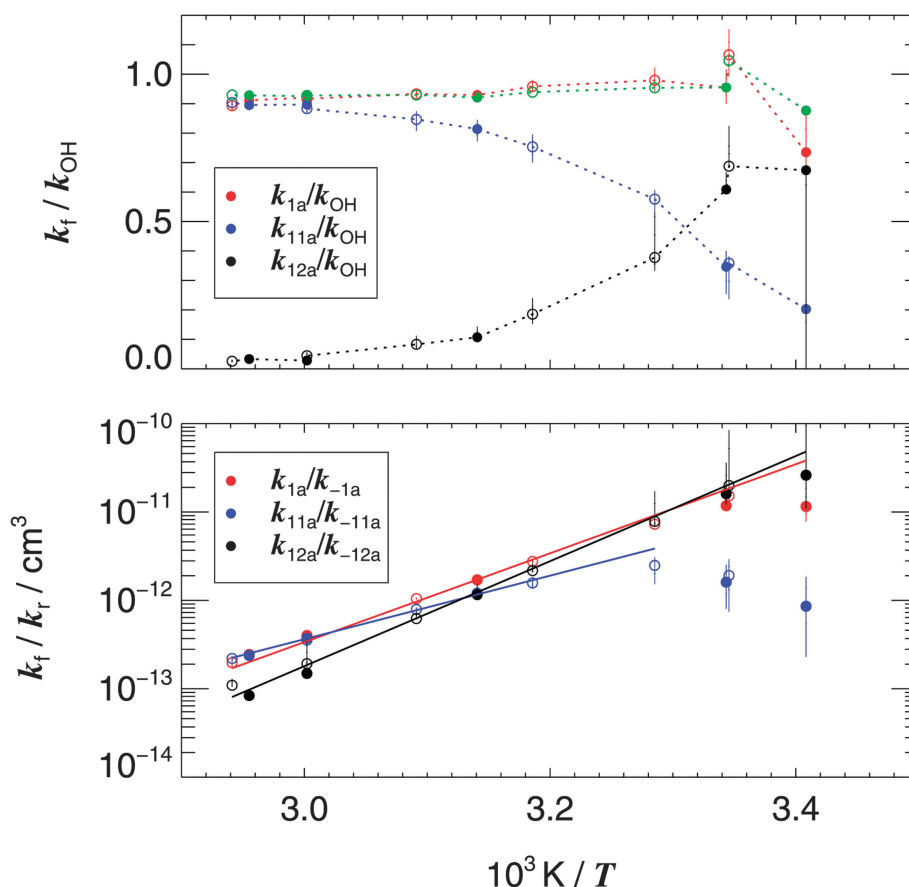This journal is © the Owner Societies 2012

Fig. 3 Adduct yields (upper panel) and equilibrium constants (lower panel) of forward and reverse reaction rate constants of the OH + 1,3,5-TMB reactions using optimized adduct background loss rate constants from the OH balance (eqn (26) and (27)). Open symbols refer to measurements at 380 mbar and filled symbols at 750 mbar. Red: model-1, blue and black: model-2. Green points in the upper panel correspond to the total of blue and black points and dashed lines simply connect the data points. Full lines in the lower panel correspond to fitted, modified van't Hoff expressions (Table 6).

and consistent with the other background loss rate constants. The upper panel of Fig. 3 shows the obtained adduct yields. The yield for model-1 varies around 0.95 as expected because of the optimized k_3. The same applies for the total adduct yield of model-2 (green points). On the other hand, the yields of add_1 and add_2 clearly show an opposite and strongly changing behaviour with add_1 prevailing above about 305 K and add_2 at lower temperatures. At the highest temperature of about 340 K, add_1 is formed almost exclusively. The same seems to be the case for add_2 at the lowest temperatures, but the contributions at lower temperatures are rather uncertain because of the uncertainties of adduct background loss rate constants, in particular k_{31}. Despite these systematic uncertainties that depend on the interpretation of k_{add}, the error limits in Fig. 3 are relatively small because they result from the mutual dependencies of the originally fitted parameters rather than the error limits in Tables 1 and 2. In accordance with the correlation coefficients obtained in simulated experiments (Section S5.3, ESI†) it was found that the maximum values of $k_f k_r$ always corresponded to maximum values of k_{OH} and k_{add} and *vice versa*. Anyway, if the model-2 approach were correct and add_2 were indeed the *ipso*-isomer, as speculated above, it would be a significant, or even the dominant product of the OH + 1,3,5-TMB reaction at room temperature and under atmospheric conditions.

To determine the stability of the adduct isomers we calculated the equilibrium constants K_c of the forward and reverse reactions. In the case of model-1:

$$K_c = \frac{k_f}{k_r} = \frac{k_{1a}}{k_{-1a}} = \frac{k_{1a}k_{-1a}}{k_{-1a}^2} = \frac{k_{1a}k_{-1a}}{(k_{add} - k_3)^2} \qquad (28)$$

For model-2:

$$K_{c1} = \frac{k_{11a}}{k_{-11a}} = \frac{k_{11a}k_{-11a}}{(k_{add_1} - k_{31})^2} \qquad (29)$$

$$K_{c2} = \frac{k_{12a}}{k_{-12a}} = \frac{k_{12a}k_{-12a}}{(k_{add_2} - k_{32})^2} \qquad (30)$$

Taking into account the reaction stoichiometry, K_c can be related to the standard reaction enthalpy $\Delta H_{r,m}^{\ominus}$ of adduct formation:

$$K_c = \frac{k_f}{k_r} = \frac{kT}{p^{\ominus}} \exp(-\Delta H_{r,m}^{\ominus}/RT + \Delta S_{r,m}^{\ominus}/R)$$

$$\propto T \exp(-\Delta H_{r,m}^{\ominus}/RT) \qquad (31)$$

In this equation $\Delta S_{r,m}^{\ominus}$ is the standard reaction entropy, k is the Boltzmann constant, R is the gas constant and $p^{\ominus}$ the standard pressure. In a narrow temperature range this

corresponds to an exponential dependence of K_c on temperature in good approximation. Nevertheless, we fitted the ratios to a modified Arrhenius, or in this case van't Hoff expression, $k_f/k_r = A_4 T \exp(-B_4/T)$ according to eqn (31). For consistency reasons we used the same optimized k_3, k_{31} and k_{32} as before for the calculations of the adduct yields.

In the lower panel of Fig. 3 the K_c are plotted as a function of reciprocal temperatures, together with the fitted functions. For model-1 and add$_2$ of model-2 the ratios show a linear behaviour in the semi-logarithmic plots. But in the case of add$_1$ of model-2 the ratio drops strongly at low temperatures (<300 K). The fit was therefore confined to a temperature range ≥ 304 K. If k_{31} were increased to a value of about 8 s^{-1} as implied by the C-result of the empirical description in Table 4, the ratios for add$_1$ at low temperatures would be greater and more consistent with a linear dependence in Fig. 3 while the slope would approach that of model-1. However, as mentioned above, greater values of k_{31} are inconsistent with the measured k_{OH}.

The fitted parameters A_4 and B_4 are given in Table 6 together with the calculated reaction enthalpies and entropies. The results for model-1 again lie in between those of model-2. For model-2 the formation enthalpy of add$_1$ of -72 ± 6 kJ mol^{-1} compares very favorably with a value of -69 ± 20 kJ mol^{-1} estimated by Perry et al.[26] for methyl-substituted benzenes including TMBs. Formation of add$_2$ is significantly more exothermic: -116 ± 8 kJ mol^{-1}. Theoretically greater reaction enthalpies were indeed predicted for ipso-type adducts by Uc et al.[8] compared to ortho-, meta- and para-adducts in the case of toluene. However, the differences were minor and generally less than 20%. In other theoretical studies ortho-adducts were slightly favored energetically in the case of toluene[33,34] and p-xylene[35] but the differences were again minor and significant yields of ipso-adducts were predicted in all cases. Andino and Vivier-Bunge[36] give an overview on currently available theoretical studies on OH-aromatic adduct isomers.

The main problem with the result for add$_2$ obtained here is that the negative reaction enthalpy is almost a factor of three greater than the activation energy for the reverse adduct dissociation (compare B_2 and B_4 in Tables 4 and 6) which is clearly inconsistent. Moreover, the reaction entropy for add$_2$ formation is almost a factor of three greater than that for add$_1$ and about a factor of two greater than a theoretically

calculated value of -101 J mol^{-1} K^{-1} for the OH-benzene adduct[37] that should be in the same range. Taking also into account the unusually low factor A_2 for add$_2$ (Table 4) and the deviations of K_{c1} from the expected dependence at low temperatures (Fig. 3), we conclude that, despite the improved fit quality compared with model-1, also model-2 is inadequate.

3.4 Model-3 with pure isomerization and intermediate cases

To find out if an adduct isomerization can resolve the inconsistencies of model-2, fits to decay curves were also performed according to model-3 with the product $k_{12a} k_{-12a}$ set to zero. Consequently, a direct formation of add$_2$ and its dissociation back to OH were deactivated while the product $k_{12} k_{21}$ was optimized. It turned out that the fitted curves and therefore also the fit qualities were identical to those of model-2. The same applies for the k_2 and the k_{OH} that we also identical. Thus from the OH decays alone we are unable to distinguish between an isomerization add$_1 \rightarrow$ add$_2$ and a direct formation OH + aromatic $\rightarrow$ add$_2$. Consequently, a full fit where all seven rate constant related parameters of model-3 are optimized simultaneously was not sensible because any intermediate case between the two extremes, i.e. $k_{12a} k_{-12a} = 0$ as assumed here and $k_{12} k_{21} = 0$ (model-2), would also explain the OH decays. This can be rationalized in terms of the parameters s, t and u in eqn (9), (21) and (22) that determine

Table 7 Model-3 fit results and estimated error limits from simultaneous triexponential fits to m decay curves at different 1,3,5-TMB concentrations (see Table 1 for m and experimental conditions). The parameters k_2, $k_{11a} + k_{12a} + k_{1b}$, DOF and χ^2/DOF are identical to those in Table 2. The product $k_{12a}k_{-12a}$ was set to zero

#	$k_{11a}k_{-11a}/$ 10^{-10} cm^3 s^{-2}	$k_{-11a} + k_{12}$ $+ k_{31}/$s^{-1}	$k_{21} + k_{32}/$s^{-1}	$k_{12}k_{21}/$s^{-2}
4	$2.5 \, ^{0.88}_{0.55}$	$12.6 \pm ^{11}_{4.5}$	$6.6 \pm ^{9.6}_{4.3}$	$30 \pm ^{159}_{26}$
5	$3.2 \, ^{0.57}_{0.40}$	$10.1 \pm ^{4.2}_{2.1}$	$5.9 \pm ^{6.0}_{3.0}$	$14 \pm ^{48}_{11}$
6	$3.5 \, ^{0.58}_{0.43}$	$11.7 \pm ^{3.9}_{2.3}$	$6.3 \pm ^{4.3}_{2.8}$	$18 \pm ^{39}_{12}$
7	$5.1 \, ^{0.60}_{0.49}$	$13.5 \pm ^{2.6}_{1.7}$	$5.7 \pm ^{4.1}_{2.5}$	$11 \pm ^{22}_{7}$
8	$11.2 \, ^{1.0}_{0.86}$	$26.4 \pm ^{2.3}_{1.9}$	$7.2 \pm ^{2.7}_{2.0}$	$17 \pm ^{16}_{8}$
9	$18.2 \, ^{2.3}_{1.9}$	$39.0 \pm ^{3.7}_{2.8}$	$7.5 \pm ^{3.6}_{2.4}$	$18 \pm ^{21}_{9}$
10	$27.3 \, ^{4.9}_{3.9}$	$59.0 \pm ^{6.8}_{5.4}$	$9.6 \pm ^{4.4}_{3.1}$	$30 \pm ^{36}_{16}$
11	$55.1 \, ^{17}_{13}$	$125 \pm ^{17}_{14}$	$13.7 \pm ^{6.3}_{4.4}$	$56 \pm ^{70}_{31}$
12	$50.1 \, ^{20}_{13}$	$117 \pm ^{22}_{15}$	$11.0 \pm ^{14}_{6.7}$	$26 \pm ^{116}_{21}$
13	$99.6 \, ^{34}_{25}$	$205 \pm ^{29}_{24}$	$23.8 \pm ^{11}_{8.4}$	$124 \pm ^{320}_{75}$
14	$107 \, ^{46}_{33}$	$221 \pm ^{34}_{29}$	$14.7 \pm ^{7.0}_{4.9}$	$67 \pm ^{79}_{36}$

Table 6 Parameters A_4 and B_4 from fitted, modified van't Hoff expressions $k_f/k_r = A_4 T \exp(-B_4/T)$ to ratios of forward and reverse rate constants k_f/k_r, standard reaction enthalpies $\Delta H_{r,m}^{\ominus}$, and reaction entropies $\Delta S_{r,m}^{\ominus}$ for the adduct formation reactions for 1,3,5-TMB. For model-1: $k_f/k_r = k_{1a}/k_{-1a}$. For model-2: $k_f/k_r = k_{11a}/k_{-11a}$ (add$_1$) and $k_f/k_r = k_{12a}/k_{-12a}$ (add$_2$). For model-3: $k_f/k_r = k_{11a}/k_{-11a}$ (add$_1$) and $k_f/k_r = k_{12}/k_{21}$ (add$_1 \rightleftharpoons$ add$_2$). Reaction enthalpies correspond to the product $R B_4$, reaction entropies to the product $R \ln(7.242 \times 10^{21}$ cm^{-3} K A_4)

k_f/k_r	A_4/cm^3 K^{-1}	B_4/10^3 K[a]	$\Delta H_{r,m}^{\ominus}$/kJ mol^{-1}	$\Delta S_{r,m}^{\ominus}$/J mol^{-1} K^{-1}
Mod-1	3.2×10^{-29}	-11.9 ± 1.3	-99 ± 11	-127 ± 15
Mod-2, add$_1$[b]	6.8×10^{-27}	-8.6 ± 0.7	-72 ± 6	-82 ± 15
Mod-2, add$_2$	3.1×10^{-34}	-14.0 ± 1.0	-116 ± 8	-223 ± 21
Mod-3, add$_1$	1.1×10^{-28}	-10.0 ± 0.8	-83 ± 7	-117 ± 19
Mod-3, add$_1 \rightleftharpoons$ add$_2$	A_4[c] 1.5×10^{-6}	-4.2 ± 2.7	-35 ± 22	-111 ± 66[d]

[a] Error limit estimated from fits to maximum and minimum k_f/k_r. [b] $T \geq 304$ K. [c] Dimensionless, fit to normal exponential van't Hoff expression. [d] Calculated from the product $R \ln(A_4)$.

13944 | Phys. Chem. Chem. Phys., 2012, **14**, 13933–13948

This journal is © the Owner Societies 2012

the same optimized decay curves. Except for $a = k_2 + k_{OH}$, the quantities $d + g = k_{add_1} + k_{add_2}$, $(bc + ef)/[\text{aromatic}] = k_{11a}\,k_{-11a} + k_{12a}\,k_{-12a}$ and $dg - hi = k_{add_1}k_{add_2} - k_{21}k_{12}$ are constant as can be verified by comparison of the data in Tables 2 and 7.

In Table 7 the fit parameters that were different for model-3 were listed. These results are also plotted in Fig. 4 as a function of reciprocal temperatures in comparison with those obtained with model-2. The differences for the two k_{add} and $k_{11a}\,k_{-11a}$ were minor which is also reflected in the similar empirical parameters A_2, B_2 and A_3, B_3 in

Tables 4 and 5, respectively. However, the interpretation of the adduct loss rate constants is different here: $k_{add_1} = k_{-11a} + k_{12} + k_{31}$ and $k_{add_2} = k_{21} + k_{32}$.

We again determined optimized k_{31}, k_{32} and the total $k_{12} + k_{31}$ by consulting the OH reaction balance similar to eqn (27):

$$k_{11a} = k_{OH} - k_{1b} = \frac{k_{11a}k_{-11a}}{k_{add_1} - k_{12} - k_{31}} \tag{32}$$

$$= \frac{k_{11a}k_{-11a}(k_{add_2} - k_{32})}{(k_{add_1} - k_{31})(k_{add_2} - k_{32}) - k_{12}k_{21}} \tag{33}$$
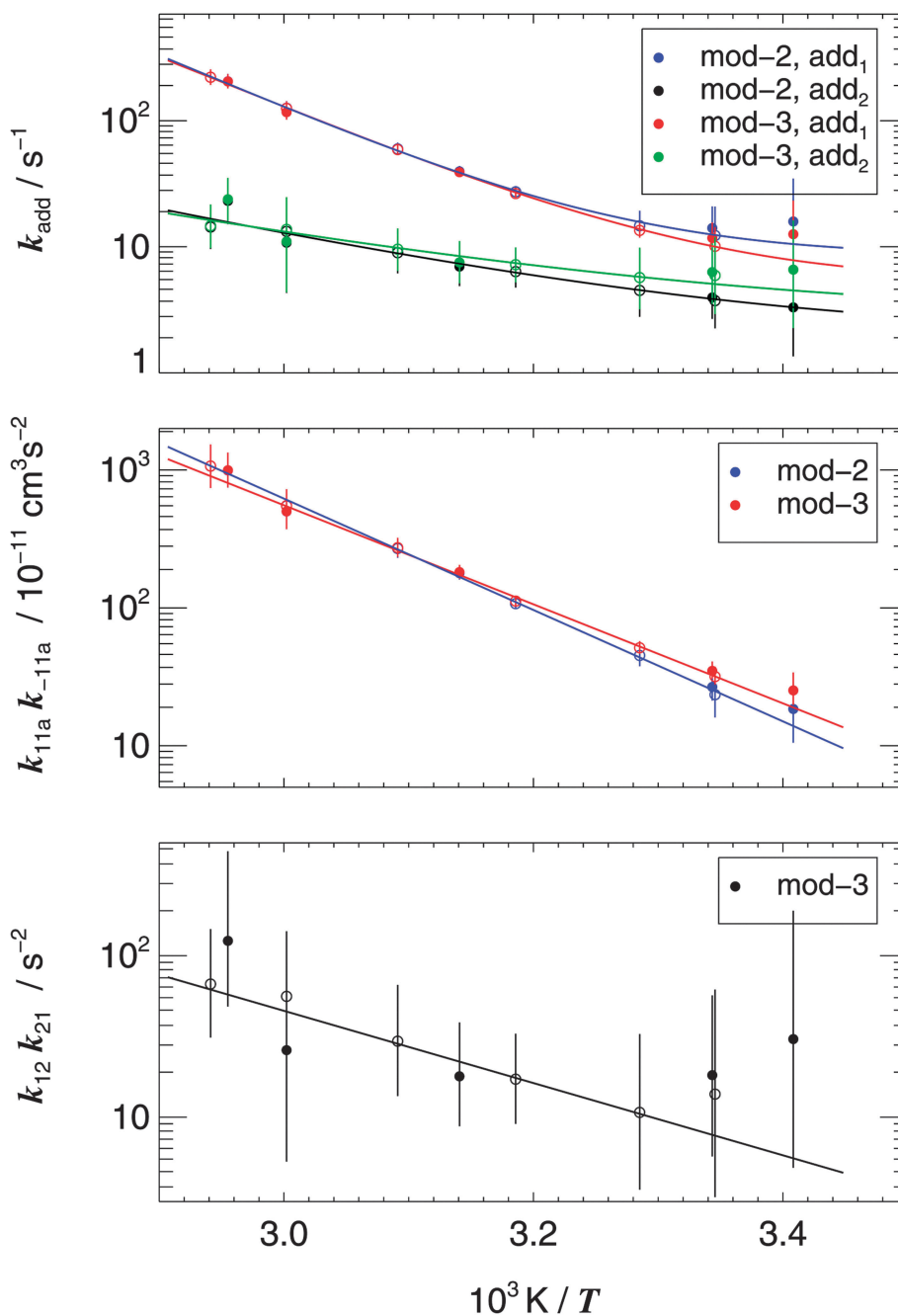

Fig. 4 Rate constant related fit parameters for 1,3,5-TMB from model-2 (blue, black) and model-3 (red, green). Open symbols refer to measurements at 380 mbar and filled symbols at 750 mbar. Full lines correspond to fitted Arrhenius expressions (Tables 4 and 5). In the first panel temperature independent contributions of background loss rate constants were assumed. Black data points in the third panel correspond to model-3.

$k_{31} = 0.6$ s^{-1}, $k_{32} = 2.7$ s^{-1} and $k_{12} + k_{31} = 5.1$ s^{-1} were obtained this way. The latter two rate constants are in good agreement with the empirical parameters C in Table 4.

With these optimized rate constants, equilibrium constants were calculated for the formation of add$_1$ in the OH reaction,

$$K_{c1} = \frac{k_{11a}}{k_{-11a}} = \frac{k_{11a} k_{-11a}}{(k_{add_1} - k_{12} - k_{31})^2} \quad (34)$$

and for formation of add$_2$ by isomerization:

$$K_{c2} = \frac{k_{12}}{k_{21}} = \frac{k_{12} k_{21}}{(k_{add_2} - k_{32})^2} \quad (35)$$

The K_{c1} were then evaluated as before according to eqn (31). The corresponding plot is shown in the upper panel of Fig. 5. Expectedly, the resulting reaction enthalpy of -83 ± 7 kJ mol^{-1} is similar to that obtained with model-2 within the combined error limits (Table 6) whilst the reaction entropies are slightly different and are both in fair agreement with the theoretical result for benzene.[37]

For the K_{c2} the factor $kT/p^{\ominus}$ in eqn (31) does not apply because of the $1:1$ stoichiometry of the isomerization reaction. A normal van't Hoff exponential fit was therefore made to obtain the reaction enthalpy of the isomerization add$_1 \rightarrow$ add$_2$ as shown in the lower panel of Fig. 5. The

corresponding value is -35 ± 22 kJ mol^{-1}. From this result, together with that for the formation of add$_1$, a reaction enthalpy of -120 ± 30 kJ mol^{-1} was calculated for add$_2$ formation. Except for the greater uncertainty, that was estimated conservatively, this enthalpy is also the same as from model-2 although the underlying reaction mechanism is different. We maintain the assumption that the more stable add$_2$ corresponds to the *ipso*-isomer.

The reaction entropy for the isomerization is smaller than the theoretically expected value that is close to zero. Nevertheless, the overall result of model-3 is more consistent than that of model-2 because the relatively small value of parameter B_2 (add$_2$ loss rate constant) now corresponds to the activation energy of the isomerization rather than of adduct dissociation. Moreover, also the low preexponential factor is explainable for the isomerization if the reaction proceeds on a non-adiabatic pathway. To our knowledge the isomerization reactions have not yet been evaluated in detail theoretically but Uc *et al.*[8] mention the possibility and a potential catalysis by O$_2$. Andino and Vivier-Bunge[36] indicate the existence of a high activation energy of about 90 kJ mol^{-1} for the *ipso* $\rightarrow$ *ortho*-isomerization that is in qualitative agreement with our result. On the other hand, the results obtained here with model-3 imply that the *ortho* $\rightarrow$ *ipso*-isomerization is a slow process (≈ 4 s^{-1}) with little if any activation energy.
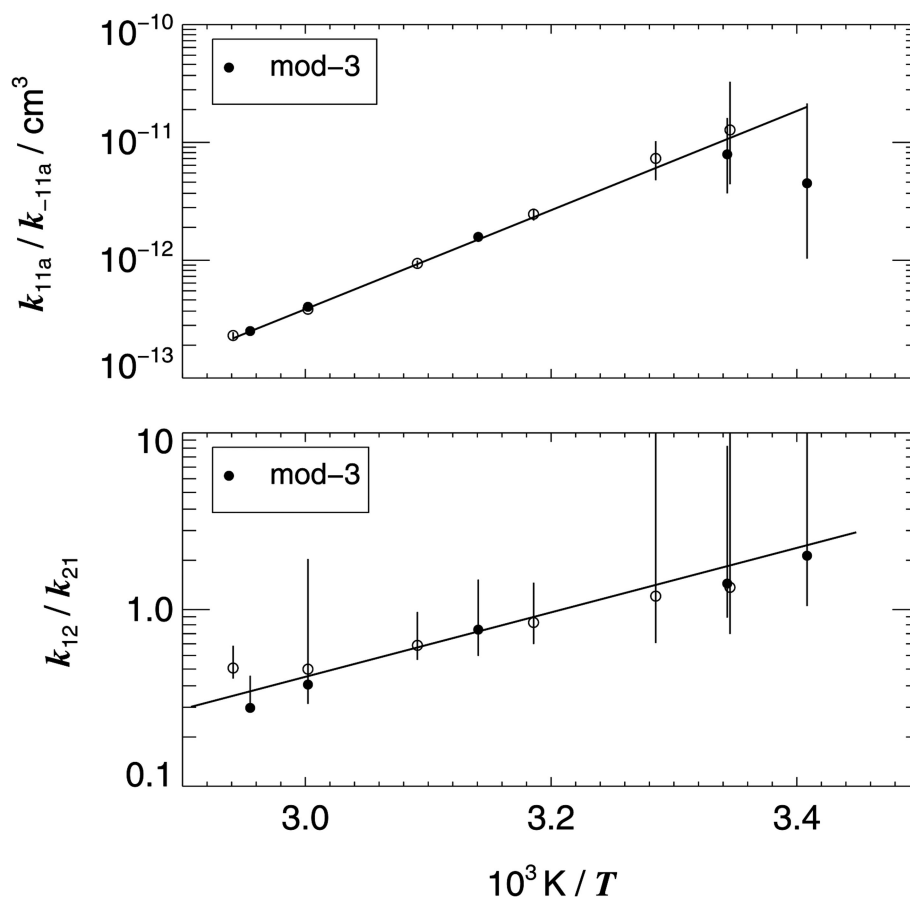

Fig. 5 Equilibrium constants for the OH + 1,3,5-TMB reaction and adduct isomerization from model-3. Open symbols refer to measurements at 380 mbar and filled symbols at 750 mbar. Full lines are fits to a modified van't Hoff expression (upper panel) and a normal van't Hoff expression (lower panel). The corresponding parameters can be found in Table 6.

Presumably, the true reaction mechanism is a mixture of the limiting cases discussed so far. A slow, underlying dissociation of add_2 back to OH + aromatic, e.g. similar to that observed for HMB,[29] would leave room for a direct formation of add_2 in the OH reaction. This is very likely, given the fast reaction of OH with HMB determined by Berndt and Böge.[9] Moreover, a contribution of adduct dissociation to k_{add_2} would weaken the decrease of the equilibrium constant K_{c2} towards higher temperatures (Fig. 5) thereby decreasing the reaction enthalpy and increasing the reaction entropy of the isomerization towards the theoretically expected value. In addition, this would lead to greater values of k_{12} with increasing temperature which means that probably both isomerization reactions are slow processes with low activation energies. That points towards a complex mechanism, e.g. via cyclic epoxy-type intermediates.

It should be noted that also catalyzed isomerizations of the type:

$$add_1 + aromatic \rightleftharpoons add_2 + aromatic$$
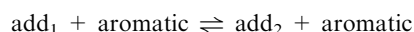
could be operative. These reactions would produce a different aromatic concentration dependence compared to model-3 and were included in the analytical treatment for two selected temperatures. However, no improvement of fit qualities was achieved by applying a corresponding dependence of the parameter hi on [aromatic]. Thus, we find no indication that these exchange reactions are of importance under our experimental conditions.

Based on the available data of this work, obviously no final conclusion can be drawn regarding the primary yields of the adducts in the OH reaction. This is unfortunate because for the atmospheric degradation of 1,3,5-TMB these primary yields are probably important. The reason is that neither the dissociation of the adducts back to OH nor an isomerization with rate constants as estimated in this work, i.e. $\leq 5 \text{ s}^{-1}$, can compete with the fast secondary reaction of the adducts with O_2 under atmospheric conditions. On the other hand, the oxygen itself could influence the isomerization and atmospheric product yields. Clearly more work is needed to elucidate the details of the mechanism. Theoretical calculations could help to clarify the discrepancy between the apparently low yield of the ipso-isomer consistently obtained here with model-2 and model-3 at temperatures > 310 K and the fast rate constant of OH reaction with hexamethylbenzene. High quality measurements with other compounds that are expected to behave similarly, e.g. 1,2,4,5-tetramethylbenzene could lead to more conclusive results. Finally there may be other, more direct methods to determine the primary yields of the adduct isomers.

4 Conclusions

OH decay curves in the presence of 1,3,5-trimethylbenzene were analysed in terms of a reaction model with reversible formation of OH-aromatic adducts leading to slow regeneration of OH. In contrast to previous studies, we examined the possibility of formation of two adduct isomers, namely ortho- and ipso-type OH-aromatic adducts as predicted theoretically. The mechanism was extended accordingly and analytical solutions were derived to fit the corresponding triexponential OH decay curves. Compared to the previous approach with only one adduct species and biexponential decay curves, the extended mechanism led to significant improvements of fit qualities, supporting formation of two adduct isomers. Moreover, the OH rate constants were different and in better agreement with literature data. Similar differences were found for the rate constants of OH + 1,2,3-trimethylbenzene and 1,2,4-trimethylbenzene. The results based on the extended mechanism are therefore preferred for all three aromatic compounds and corresponding Arrhenius expressions were derived.

Formation of adduct isomers was studied in detail for 1,3,5-trimethylbenzene. The apparent kinetic properties of the adduct isomers were strongly different but the calculated thermochemical data for formation and dissociation of the more stable adduct isomer were contradictory. An alternative mechanism was therefore tested where the second isomer is formed by isomerization instead of the OH reaction. This led to the same fit functions but more consistent thermochemical results with reaction enthalpies of $-83 \pm 7 \text{ kJ mol}^{-1}$ and $-35 \pm 22 \text{ kJ mol}^{-1}$ for the formation of one adduct isomer and the isomerization into the other, respectively. Based on a comparison with literature results for benzene and hexamethylbenzene, the more stable adduct was assigned to the ipso-adduct. An intermediate mechanism with formation of both adducts by OH reaction and isomerization is likely but cannot be further specified based on the available data.

Acknowledgements

References

1 J. G. Calvert, R. Atkinson, K. H. Becker, R. M. Kamens, J. H. Seinfeld, T. J. Wallington and G. Yarwood, Mechanisms of atmospheric oxidation of aromatic hydrocarbons, Oxford University Press, 2002.
2 R. Atkinson and J. Arey, Chem. Rev., 2003, 103, 4605–4638.
3 R. Atkinson and J. Arey, Polycyclic Aromat. Compd., 2007, 27, 15–40.
4 A. Wahner and C. Zetzsch, J. Phys. Chem., 1983, 87, 4945–4951.
5 F. Witte, E. Urbanik and C. Zetzsch, J. Phys. Chem., 1986, 90, 3251–3259.
6 R. Knispel, R. Koch, M. Siese and C. Zetzsch, Ber. Bunsen-Ges., 1990, 94, 1375–1379.
7 R. Koch, R. Knispel, M. Elend, M. Siese and C. Zetzsch, Atmos. Chem. Phys., 2007, 7, 2057–2071.
8 V. H. Uc, I. Garcia-Cruz, A. Hernandez-Laguna and A. Vivier-Bunge, J. Phys. Chem. A, 2000, 104, 7847–7855.
9 T. Berndt and O. Böge, Int. J. Chem. Kinet., 2001, 33, 124–129.
10 H. Geiger, I. Barnes, K. H. Becker, B. Bohn, T. Brauers, B. Donner, H. P. Dorn, M. Elend, C. M. F. Dinis, D. Grossmann, H. Hass, H. Hein, A. Hoffmann, L. Hoppe, F. Hülsemann, D. Kley, B. Klotz, H. G. Libuda, T. Maurer, D. Mihelcic, G. Moortgat, R. Olariu, P. Neeb, D. Poppe, L. Ruppert, C. G. Sauer, O. Shestakov, H. Somnitz, W. R. Stockwell, L. P. Thüner, A. Wahner, P. Wiesen, F. Zabel, R. Zellner and C. Zetzsch, J. Atmos. Chem., 2002, 42, 323–357.

This journal is © the Owner Societies 2012

Phys. Chem. Chem. Phys., 2012, 14, 13933–13948 | 13947

11 F. Stuhl and H. Niki, *J. Chem. Phys.*, 1972, **57**, 3671–3677.
12 F. Stuhl and H. Niki, *J. Chem. Phys.*, 1972, **57**, 3677–3679.
13 R. Koch, *PhD thesis*, University of Hannover, 1992.
14 R. Knispel, *PhD thesis*, University of Hannover, 1993.
15 E. R. Hopke and G. W. Sears, *J. Am. Chem. Soc.*, 1948, **70**, 3801–3803.
16 R. M. Stephenson, S. Malanowski and D. Ambrose, *Handbook of the thermodynamics of organic compounds*, Elsevier, 1987.
17 S. Zhang and C. Zetzsch, *Gas Kinetics Conference 2010*, 2010.
18 S. P. Sander, J. Abbatt, J. R. Barker, J. B. Burkholder, R. R. Friedl, D. M. Golden, R. E. Huie, C. E. Kolb, M. J. Kurylo, G. K. Moortgat, V. L. Orkin and P. H. Wine, *Chemical kinetics and photochemical data for use in atmospheric studies, Evaluation No. 17*, Jet Propulsion Laboratory, Pasadena, 2011 http://jpldataeval.jpl.nasa.gov, 2011.
19 A. Bolovinos, J. Philis, E. Pantos, P. Tsekeris and G. Andritsopoulos, *J. Chem. Phys.*, 1981, **75**, 4343–4349.
20 A. Bolovinos, J. Philis, E. Pantos, P. Tsekeris and G. Andritsopoulos, *J. Mol. Spectrosc.*, 1982, **94**, 55–68.
21 R. A. Alberty, *J. Chem. Educ.*, 2004, **81**, 1206–1209.
22 R. Atkinson, *J. Phys. Chem. Ref. Data*, 1989, **Monograph 1** 204.
23 C. Markwardt, IDL Library, http://cow.physics.wisc.edu/~craigm/idl/, 2010.
24 S. Nehr, B. Bohn, H. Fuchs, A. Hofzumahaus and A. Wahner, *Phys. Chem. Chem. Phys.*, 2011, **13**, 10699–10708.
25 D. A. Hansen, R. Atkinson and J. N. Pitts, *J. Phys. Chem.*, 1975, **79**, 1763–1766.
26 R. A. Perry, R. Atkinson and J. N. Pitts, *J. Phys. Chem.*, 1977, **81**, 296–304.
27 S. M. Aschmann, W. D. Long and R. Atkinson, *J. Phys. Chem. A*, 2006, **110**, 7393–7400.
28 M. J. Pilling and P. W. Seakins, *Reaction Kinetics*, Oxford University Press, 1996.
29 J. von Buttlar, R. Koch, M. Siese and C. Zetzsch, EGU General Assembly 2008, *Geophys. Res. Abstr. 10*, 2008, EGU2008-A-10576.
30 F. P. Tully, A. R. Ravishankara, R. L. Thompson, J. M. Nicovich, R. C. Shah, N. M. Kreutter and P. H. Wine, *J. Phys. Chem.*, 1981, **85**, 2262–2269.
31 J. M. Nicovich, R. L. Thompson and A. R. Ravishankara, *J. Phys. Chem.*, 1981, **85**, 2913–2916.
32 IUPAC Subcommittee on gas kinetic data evaluation, http://www.iupac-kinetic.ch.cam.ac.uk/, 2008.
33 I. Suh, D. Zhang, R. Zhang, L. T. Molina and M. J. Molina, *Chem. Phys. Lett.*, 2002, **364**, 454–462.
34 D. Johnson, S. Raoult, R. Lesclaux and L. N. Krasnoperov, *J. Photochem. Photobiol., A*, 2005, **176**, 98–106.
35 J. Fan and R. Zhang, *J. Phys. Chem. A*, 2006, **110**, 7728–7737.
36 J. M. Andino and A. Vivier-Bunge, *Adv. Quantum Chem.*, 2008, **55**, 297–310.
37 T. H. Lay, J. W. Bozzelli and J. H. Seinfeld, *J. Phys. Chem.*, 1996, **100**, 6543–6554.
38 R. Atkinson, S. Aschmann, J. Arey and W. Carter, *Int. J. Chem. Kinet.*, 1989, **21**, 801–827.
39 F. Kramp and S. E. Paulson, *J. Phys. Chem. A*, 1998, **102**, 2685–2690.
40 S. M. Aschmann, E. C. Tuazon and R. Atkinson, *J. Phys. Chem. A*, 2005, **109**, 2282–2291.